RETROSPECTIVE OPERATIONAL AFTERSHOCK FORECASTING FOR 2016 AMATRICE–NORCIA SEISMIC SEQUENCE IN CENTRAL ITALY

2 authors:

Hossein Ebrahimian
University of Naples Federico II
42 PUBLICATIONS   **473** CITATIONS

SEE PROFILE

F. Jalayer
University of Naples Federico II
112 PUBLICATIONS   **3,174** CITATIONS

SEE PROFILE

Some of the authors of this publication are also working on these related projects:

[ICOSSAR 2021] Mini-symposium MS23 "Nonlinear Dynamic Analysis Procedures for Seismic Risk Assessment of Civil Infrastructure: Progress and Challenges" View project

[Sustainability] Special Issue "Sustainable Assessment and Modelling in Seismic Risk Mitigation" View project

RETROSPECTIVE OPERATIONAL AFTERSHOCK FORECASTING FOR 2016 AMATRICE-NORCIA SEISMIC SEQUENCE IN CENTRAL ITALY

Hossein Ebrahimian[1], **Fatemeh Jalayer**[2]

[1] Assistant Professor
Department of Structures for Engineering and Architecture, University of Naples Federico II, Via Claudio 21, Naples 80125, Italy
e-mail: ebrahimian.hossein@unina.it

[2] Associate Professor
Department of Structures for Engineering and Architecture, University of Naples Federico II, Via Claudio 21, Naples 80125, Italy
e-mail: fatemeh.jalayer@unina.it

Abstract

The first days elapsed after the occurrence of an earthquake and its triggered aftershocks are crucial in terms of emergency decision-making. To this end, the adopted novel and fully-probabilistic procedure succeeds in providing spatio-temporal predictions of aftershock occurrence in a prescribed forecasting time interval (in the order of hours or days). The procedure aims at exploiting the information provided by the ongoing seismic sequence in quasi-real time. The versatility of the Bayesian inference is exploited to adaptively update the forecasts based on the incoming information as it becomes available. The aftershock clustering in space and time is modelled based on an Epidemic Type Aftershock Sequence (ETAS) model. One of the main novelties of the proposed procedure is that it considers the uncertainties in the aftershock occurrence model and its model parameters. This is done by pairing up the Bayesian robust reliability framework and the suitable simulation schemes (Markov Chain Monte Carlo Simulation) provides the possibility of performing the whole forecasting procedure with minimum (or no) need of human interference. This procedure is demonstrated through a retrospective spatio-temporal early forecasting of seismicity associated with the 2016 Amatrice-Norcia seismic sequence in central Italy. Seismicity forecasts are issued with various time intervals in the first few days after the main events within the sequence.

Keywords: Time-dependent reliability, Aftershock sequence, ETAS, Markov Chain Monte Carlo Simulation, Operational aftershock forecasting, Central Italy seismic sequence.

1 INTRODUCTION

Short-term operational seismicity forecasts (in the order of days to months), in the presence of a vast number of aftershocks following a large earthquake, are of utmost importance for emergency decision-making and risk mitigation in the disaster area [[1]-4]. The Epidemic Type Aftershock Sequence (ETAS) model [5, 6] is the stochastic model most frequently used to describe earthquake occurrence within a seismic sequence. It is an epidemic stochastic point process in which every earthquake within the sequence is a potential triggering event for subsequent earthquakes, and therefore generates its own well-defined Modified Omori [7] (MO) aftershock decay. Hence, it is capable of accounting for the triggering effect of all the events that have taken place before a desired time. The ETAS model performed quite well in operational seismic forecasting during the L'Aquila 2009 (central Italy) seismic sequence [8]. The model parameters are usually calibrated a priori based on the maximum likelihood criterion. The first effort on the calibration of temporal model parameters has been carried in [5], and extended later [6, 9, 10] to estimate the spatio-temporal model parameters. In addition, several attempts are made for developing improved algorithms to attain maximum likelihood estimates of ETAS parameters [11-13]. Adaptive model parameter estimation based on the events in the ongoing sequence (e.g., calibrating the parameters of MO and ETAS models based on the ongoing catalogue by employing Bayesian parameter estimation [14-18]) has the advantage of both tuning a sequence-specific model, and also capturing possible time variations of the model parameters. As the original purpose of the present paper, we propose a fully simulation-based method to provide a *robust estimate* [16, 18] for the spatial distribution of the events in a prescribed forecasting time interval after the main event. In the context of this robust estimate, the uncertainty in the ETAS model parameters is taken into account as the posterior joint probability distribution for the model parameters conditioned on the events that have already occurred (i.e., registered events in the ongoing seismic sequence before the beginning of the forecasting interval). The Markov Chain Monte Carlo (MCMC) simulation scheme [16-19] is used to sample directly from the posterior probability distribution for ETAS model parameters (i.e., conditioned on the registered events in the ongoing sequence). Moreover, this robust estimate also considers the sequence of events that is going to occur during the forecasting interval (and hence affect the seismicity in an epidemic type model like ETAS). Although this sequence is unknown at the time of forecasting, we propose a stochastic procedure to generate it. The procedure leads to the stochastic spatio-temporal distribution of the forecasted events and consequently to the uncertainty in the estimated number of events, corresponding to a given forecasting interval. The resulting robust forecasts are directly applicable in adaptive daily aftershock hazard and risk assessment procedures [15, 20-22].

The proposed methodology is applied to provide retrospective early forecasting of seismicity associated with the 2016 Amatrice seismic sequence activities in central Italy. Robust spatio-temporal short-term seismicity forecasts are provided with various time intervals in the first few days elapsed after main events within the sequence, which can predict the seismicity within plus/minus two standard deviations from the mean estimate within the few hours elapsed after the main event.

2 METHODOLOGY

The aftershock occurrence is described herein by a non-homogenous Poisson point process over the two-dimensional space and time. Hence, the aftershock zone can be described as the set A in the Cartesian space discretized into mutually exclusive and collectively exhaustive (MECE) subsets or spatial cell units centered at $(x,y) \in A$. In this manner, $\lambda(t,x,y,m|\mathbf{seq},M_l)$ represents the rate of occurrence of events in the forecasting interval $[T_{start},T_{end}]$ at time t

elapsed after the main event (a.k.a. main-shock) occurred at time of origin T_o with magnitude greater than or equal to m and in the cell unit centered at $(x,y) \in A$, given (a) the observation history **seq** which is the sequence of N_o events (including main-shock and the sequence of aftershocks) taken place before the forecasting interval (i.e. in the interval $[T_o , T_{start})$), and (b) the lower cut-off magnitude M_l. Hence, **seq** can be expressed as $\mathbf{seq} = \{(t_i, x_i, y_i, m_i), t_i < T_{start}, m_i \geq M_l, i=1:N_o\}$, where t_i is the arrival time for the ith event with magnitude M_i and location $(x_i, y_i) \in A$. The average number of events in the spatial cell unit centered at (x,y) with magnitude greater than or equal to m in the forecasting interval $[T_{start}, T_{end}]$ can then be calculated as:

$$N(x,y,m|\mathbf{seq}, M_l) = N_b(x,y,m|M_l) + \int_{T_{start}}^{T_{end}} \lambda(t,x,y,m|\mathbf{seq}, M_l) \, dt \tag{1}$$

where $N_b(x,y,m|M_l)$ is a constant representing the background seismicity of the area. Let $\boldsymbol{\theta}$ denote the vector of model parameters for $\lambda(t,x,y,m|\mathbf{seq},M_l)$. Given a particular space-time model and a realization of the vector of model parameters $\boldsymbol{\theta}$, one can calculate a plausible value for the rate of occurrence denoted as $\lambda(t,x,y,m|\boldsymbol{\theta},\mathbf{seq},M_l)$. A robust estimate [16, 18, 19, 23] of the average number of events in the spatial cell unit centered at (x,y) with magnitude greater than or equal to m in the forecasting interval $[T_{start}, T_{end}]$, and over the domain of the model parameters $\Omega_{\boldsymbol{\theta}}$ can be calculated as:

$$\mathbb{E}[N(x,y,m|\mathbf{seq}, M_l)] = N_b(x,y,m|M_l) + \int_{\Omega_{\boldsymbol{\theta}}} \int_{T_{start}}^{T_{end}} \lambda(t,x,y,m|\boldsymbol{\theta},\mathbf{seq}, M_l) \cdot p(\boldsymbol{\theta}|\mathbf{seq}, M_l) \, dt \, d\boldsymbol{\theta} \tag{2}$$

where $p(\boldsymbol{\theta}|\mathbf{seq},M_l)$ is the conditional probability distribution function (PDF) for $\boldsymbol{\theta}$ given the **seq** and the lower cut-off magnitude M_l.

As mentioned above, **seq** denotes the sequence of events taking place before the beginning of the forecasting interval (i.e., in the interval $[T_o , T_{start})$). However, the triggering effect of the events taking place during the forecasting interval $[T_{start}, T_{end}]$ is expected to play a major role. The sequence of events taking place during the forecasting interval denoted as **seqg**, which is unknown at the time of forecasts, is simulated/generated herein. Let us assume that a plausible **seqg** is defined as the events within the forecasting interval defined as $\mathbf{seqg} = \{(IAT_i, x_i, y_i, m_i), T_{start} \leq t_i \leq T_{end}, m_i \geq M_l\}$, where $IAT_i = t_i - t_{i-1}$ stands for the inter-arrival time. The robust estimate for the number of aftershock events in Eq. (2) should also consider all the plausible sequences of events **seqg** (i.e., the domain $\Omega_{\mathbf{seqg}}$) that can happen during the forecasting time interval:

$$N(x,y,m|\mathbf{seq}, M_l) = N_b(x,y,m|M_l) +$$
$$\int_{\Omega_{\boldsymbol{\theta}}} \left[\int_{\Omega_{\mathbf{seqg}}} \left(\int_{T_{start}}^{T_{end}} \lambda(t,x,y,m|\mathbf{seqg},\boldsymbol{\theta},\mathbf{seq}, M_l) \, dt \right) p(\mathbf{seqg}|\boldsymbol{\theta},\mathbf{seq}, M_l) \, d\mathbf{seqg} \right] p(\boldsymbol{\theta}|\mathbf{seq}, M_l) \, d\boldsymbol{\theta} \tag{3}$$

where $p(\mathbf{seqg}|\boldsymbol{\theta},\mathbf{seq},M_l)$ is the PDF for the generated sequence **seqg** given that $\boldsymbol{\theta}$ and **seq** are known and $\lambda(t,x,y,m|\mathbf{seqg},\boldsymbol{\theta},\mathbf{seq},M_l)$ is the space-time clustering model. Herein, we have employed the space-time clustering ETAS model considering also the sequence of events taking place within the forecasting interval.

The ETAS model is an epidemiological stochastic point process in which every earthquake is a potential triggering event for subsequent earthquakes [5, 6, 9, **Errore. L'origine riferi-**

mento non è stata trovata.0]. According to the general ETAS model, we adopt the spatio-temporal triggering effect of a given sequence on the seismicity rate, denoted as λ_{ETAS}, as:

$$\lambda_{\text{ETAS}}\left(t,x,y,m\middle|\boldsymbol{\theta},\mathbf{seq}_t,M_l\right)=e^{-\beta(m-M_l)}\sum_{t_j<t}K\,e^{\beta\left(M_j-M_l\right)}\cdot\frac{K_t}{\left(t-t_j+c\right)^p}\cdot\frac{K_R}{\left(r_j^2+d^2\right)^q} \tag{4}$$

where $\mathbf{seq}_t=\{(t_j,x_j,y_j,M_j),\ t_j<t,\ M_j\geq M_l\}$ is the observation history up to the time t; parameter β is related to Gutenberg-Richter seismicity; parameters c and p are similar to those of the Modified Omori's Law [7] defining the decay in time of short-term triggering effect; d and q characterize the spatial distribution of the triggered events; r_j is the distance between the location $(x,y)\in A$ and the epicenter of the jth event (x_j,y_j); parameters K, K_t and K_R satisfy the achievement of asymptotic compatibility between ETAS predictions and the long-term seismicity (see [18] for a comprehensive discussion on satisfying the compatibility condition for the parameters K, K_t and K_R).

Thus, the vector of model parameters $\boldsymbol{\theta}$ can be defined as $\boldsymbol{\theta}=[\beta,K,K_t,K_R,c,p,d,q]$. It is to note that parameters K, K_t, and K_R are derived as a function of other model parameters in $\boldsymbol{\theta}$; therefore, the main parameters of the ETAS model include $[\beta,c,p,d,q]$. The rate of events in the ETAS model with magnitude (exactly) equal to m, denoted herein as μ_{ETAS} herein, is calculated by taking the derivative of Eq. (4) with respect to magnitude m:

$$\mu_{\text{ETAS}}\left(t,x,y,m\mid\boldsymbol{\theta},\mathbf{seq}_t,M_l\right)=\left|\partial\lambda_{\text{ETAS}}/\partial m\right|=\beta e^{-\beta(m-M_l)}\lambda_{\text{ETAS}}\left(t,x,y,M_l\mid\boldsymbol{\theta},\mathbf{seq}_t,M_l\right) \tag{5}$$

The integral with respect to time in Eq. (3) cannot be calculated analytically over the entire interval $[T_{start},T_{end}]$, and is approximated by summing over the sub-intervals $[t_{i-1},t_i]$ within **seqg**:

$$\int_{T_{start}}^{T_{end}}\lambda\left(t,x,y,m\middle|\mathbf{seqg},\boldsymbol{\theta},\mathbf{seq},M_l\right)\mathrm{d}t=\sum_{\Omega_{\mathbf{seqg}}}\int_{t_{i-1}}^{t_i}\lambda_{\text{ETAS}}\left(t,x,y,m\mid\mathbf{seqg}_{i-1},\boldsymbol{\theta},\mathbf{seq},M_l\right)\mathrm{d}t$$

$$=\sum_{\Omega_{\mathbf{seqg}}}\left(KK_tK_R\,e^{-\beta(m-M_l)}\sum_{t_j<t_i}\frac{e^{\beta\left(M_j-M_l\right)}\mathrm{I}_0\left(t_i,t_{i-1},t_j\right)}{\left(r_j^2+d^2\right)^q}\right) \tag{6}$$

where λ_{ETAS} has the functional form presented in Eq. (4), and **seqg**$_{i-1}$ is the previous (i-1) events within the generated sequence. In the following sections, it is described first how sequence of events **seqg** for the forecasting interval is sampled based on $p(\mathbf{seqg}|\boldsymbol{\theta},\mathbf{seq},M_l)$. Later on, the method for sampling $\boldsymbol{\theta}$ from the distribution $p(\boldsymbol{\theta}|\mathbf{seq},M_l)$ is discussed.

2.1 Generating sequences according to $p(\mathbf{seqg}|\boldsymbol{\theta},\mathbf{seq},M_l)$

The probability distribution $p(\mathbf{seqg}|\boldsymbol{\theta},\mathbf{seq},M_l)$ in Eq. (3) can be written as follows [18]:

$$p\left(\mathbf{seqg}\mid\boldsymbol{\theta},\mathbf{seq},M_l\right)=\prod_i p\left(IAT_i,x_i,y_i,M_i\mid\mathbf{seqg}_{i-1},\boldsymbol{\theta},\mathbf{seq},M_l\right) \tag{7}$$

where **seqg**$_i$ is the generated sequence up to the ith event, where **seqg**$_i=\{\mathbf{seqg}_{i-1},(IAT_i,x_i,y_i,m_i)\}$, and the sequence of events that precede the ith generated event is $\{\mathbf{seq},\mathbf{seqg}_{i-1}\}$. The probability distribution $p(IAT_i,x_i,y_i,m_i|\mathbf{seqg}_{i-1},\boldsymbol{\theta},\mathbf{seq},M_l)$ can be further expanded (again using the probability product rule) as follows:

$$p(IAT_i, x_i, y_i, m_i \mid \mathbf{seqg}_{i-1}, \boldsymbol{\theta}, \mathbf{seq}, M_l) =$$
$$p(m_i \mid \mathbf{seqg}_{i-1}, \boldsymbol{\theta}, \mathbf{seq}, M_l) p(IAT_i \mid m_i, \mathbf{seqg}_{i-1}, \boldsymbol{\theta}, \mathbf{seq}, M_l) p(x_i, y_i \mid IAT_i, m_i, \mathbf{seqg}_{i-1}, \boldsymbol{\theta}, \mathbf{seq}, M_l) \quad (8)$$

where $p(m_i|\mathbf{seqg}_{i-1},\boldsymbol{\theta},\mathbf{seq},M_l)$ is the marginal PDF for the magnitude m_i given the sequence of events that precede it, $\boldsymbol{\theta}$, and M_l; $p(IAT_i|m_i,\mathbf{seqg}_{i-1},\boldsymbol{\theta},\mathbf{seq},M_l)$ is the (conditional) marginal PDF for inter-arrival time IAT_i given that the value of magnitude is equal to m_i; finally, the term $p(x_i,y_i|IAT_i,m_i,\mathbf{seqg}_{i-1},\boldsymbol{\theta},\mathbf{seq},M_l)$ is the conditional joint PDF for the spatial position $(x_i,y_i) \in A$ given that IAT_i and m_i are known. It should be noted that the break-down into the product of several conditional PDFs is necessary during the sequence generation process.

To generate a plausible sequence of events during the forecasting interval, the procedure, illustrated by the flowchart in Fig. 1 is adopted (for a comprehensive discussion on generating the ith event within the sequence **seqg**, see the steps discussed in [18]).
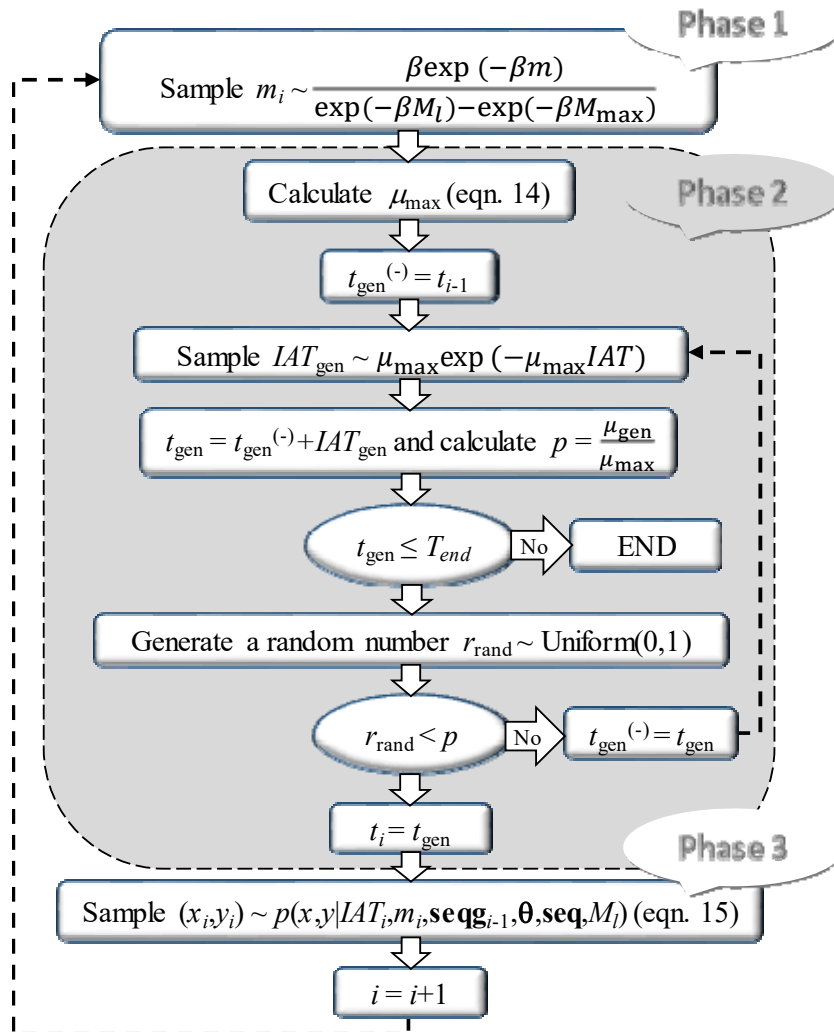
Figure 1: The flowchart for generating **seqg** (see [18] for complete discussion)

2.2 Sampling θ from the distribution $p(\boldsymbol{\theta}|\mathbf{seq},M_l)$

The probability distribution $p(\boldsymbol{\theta}|\mathbf{seq},M_l)$ in Eq. (3) can be calculated using Bayesian parameter estimation:

$$p\left(\boldsymbol{\theta}\big|\mathbf{seq}, M_l\right) = C^{-1} p\left(\mathbf{seq}\big|\boldsymbol{\theta}, M_l\right) p\left(\boldsymbol{\theta}\big|M_l\right) \tag{9}$$

where $p(\mathbf{seq}|\boldsymbol{\theta},M_l)$ denotes the likelihood of the observed sequence given the vector of model parameters $\boldsymbol{\theta}$ and lower cut-off magnitude M_l, $p(\boldsymbol{\theta}|M_l)$ is the prior distribution for the vector $\boldsymbol{\theta}$, and C^{-1} is a normalizing constant. In lieu of additional information (e.g., statistics of regional model parameters), the prior joint distribution $p(\boldsymbol{\theta}|M_l)$ can be estimated as the product of marginal uniform probability distributions for each model parameter. In order to sample from $p(\boldsymbol{\theta}|\mathbf{seq},M_l)$, Markov Chain Monte Carlo (MCMC) simulation routine is employed which is particularly useful for cases where the sampling needs to be done from a probability distribution that is known up to a constant value [19] (herein, C^{-1}). The MCMC routine uses the Metropolis-Hastings (MH) algorithm [24, 25] in order to generate samples as a Markov Chain sequence used first to sample from the target probability distribution $p(\boldsymbol{\theta}|\mathbf{seq},M_l)$, and later to estimate the robust reliability in equation (3). The MH routine is shown in Fig. 2 (see [18] for complete discussion on the MH algorithm).

The likelihood for the observed sequence $p(\mathbf{seq}|\boldsymbol{\theta},M_l)$, where $\mathbf{seq}=\{(t_i,x_i,y_i,m_i),\ t_i<T_{start},\ m_i\geq M_l,\ i=1:N_o\}$, with N_o events, including the main-shock (with $i=1$) and the sequence of aftershocks is derived in [18].
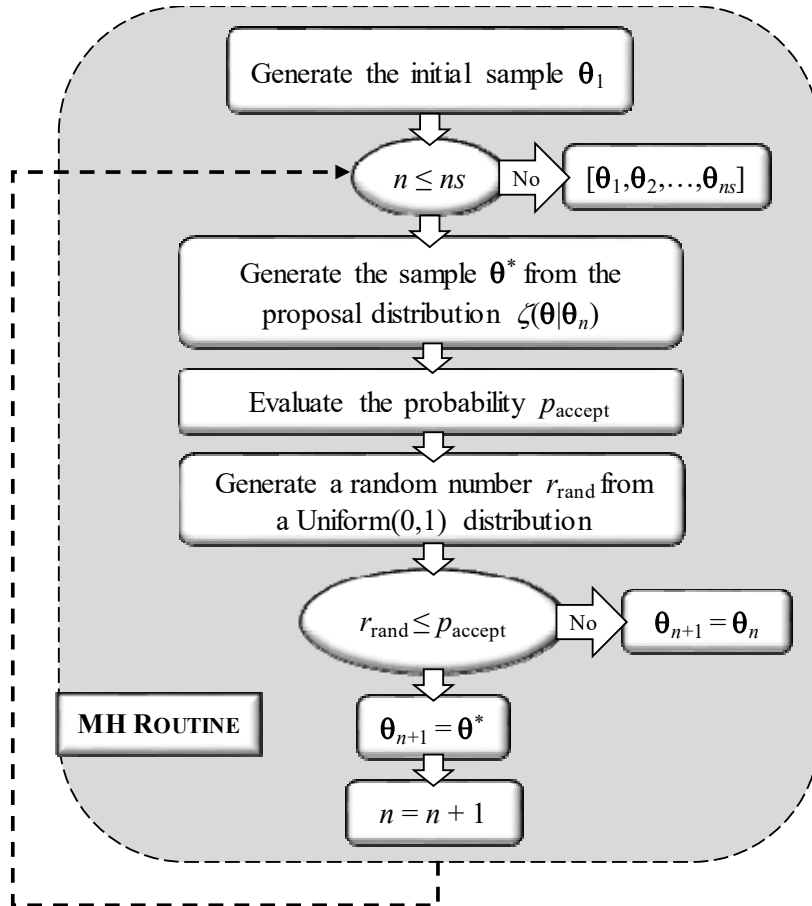
Figure 2: Metropolis-Hastings (MH) algorithm (see [18])

3   CASE-STUDY APPLICATION

3.1   Amatrice-Norcia 2016 seismic sequence

The proposed methodology presented in Section 2 is applied to provide retrospective forecasting for seismic activities of the 2016 Amatrice-Norcia sequence by analysing the registered data of quasi real-time catalogues from INGV (Istituto Nazionale di Geofisica E Vulcanologia). The corresponding aftershock zone, as shown in Fig. 3a by the gray-colored area, is located mostly within the seismic zone 923 based on the ZS9 Italian Seismogenetic Zonation [26]. Fig. 3a shows also the seismogenic zonations surrounding the aftershock zone. It is to note that based on the Italian seismic zonations, the upper-bound magnitude for seismic zone Z923 is M_{max}=7.06. On the 24th of August 2016 at 01:36 UTC, a Mw 6.0 earthquake struck the Central Italy between towns of Norcia and Amatrice, devastating Amatrice, Accumoli and several surrounding small towns and villages, causing almost 300 fatalities and leaving almost 30,000 homeless. The seismic sequence, including a Mw 5.4 aftershock (occurred almost one hour after the main shock at 02:33 UTC), triggered hundreds of earthquakes per day until the mid-September. Two months after, on the 26th of October, a Mw 5.4 followed within a two-hour delay by a Mw 5.9 earthquake (at 17:10 and 19:18 UTC, respectively) took place in the east of town Visso, and preceded the largest event of the sequence, a Mw 6.5 on October 30 at 06:40 UTC, North of Norcia. This one is the largest earthquake recorded in Italy since the Mw 6.9 1980 Irpinia event. Fig. 3b and Fig. 3c illustrate the seismic activities within the aftershock zone during the first two months highlighting the key events taken place. The present study strives to perform robust forecasts for the spatio-temporal evolution of the events in specific time intervals within the very complex sequence described above that is distinguished by three main events ("main-shocks") of moment magnitudes 6.0, 5.9, and 6.5, respectively (as illustrated in Fig. 3b). We divide the sequence into three parts: (a) from 24-August to 25-October, (b) from 26-October to 29-October, and finally (c) from 30-October to 1-November. We have used two different catalogues herein in order to gather data backwards in time (see [18]).

3.2   Daily forecasts of seismicity from August 24 up to October 25

Figure 4 shows the forecasted seismicity maps in terms of the mean plus two logarithmic standard deviation (98% confidence interval) for the number of events with $M{\geq}3.0$ within each spatial cell unit issued for the 24-hour time forecasting intervals. The prediction time window [T_{start}, T_{end}] indicates a 24-hour interval where T_{start} is 6:00 UTC of the following day. The sequence **seq** comprised of events registered in the Catalogue including the main event up to the time T_{start}. To issue the first forecast in Fig. 4a, the observation history, **seq**, comprises the main event with Mw 6.0 at 01:36 UTC and the triggered events up to 6:00 UTC of 24 August 2016, where the lower cut-off magnitude, M_l, of Catalogue is equal to 3.0 based on the two methods discussed in [15] (the procedure adopted for evaluating the completeness magnitude M_c throughout the various phases of this multiple seismic sequence is described in detail in [18]). In any case, M_l=3.0 is considered as the cut-off threshold for the computation of the aftershock rates for the upcoming days.

The first step towards providing seismicity forecasts (with reference to Eq. 3) is sampling from the distribution of modal parameters θ based on posterior (target) probability distribution $p(\theta|\mathbf{seq},M_l)$. The vector θ=[$\beta$, K, K_t, K_R, c, p, d, q] is updated on a daily basis by applying the Bayesian updating routine illustrated in Eq. (9) and considering that parameters K, K_t, K_R are derived as function of other parameters within vector θ (see [18]). Samples for θ are generated as a Markov Chain sequence directly from $p(\theta|\mathbf{seq},M_l)$, as noted in Section 2.2.
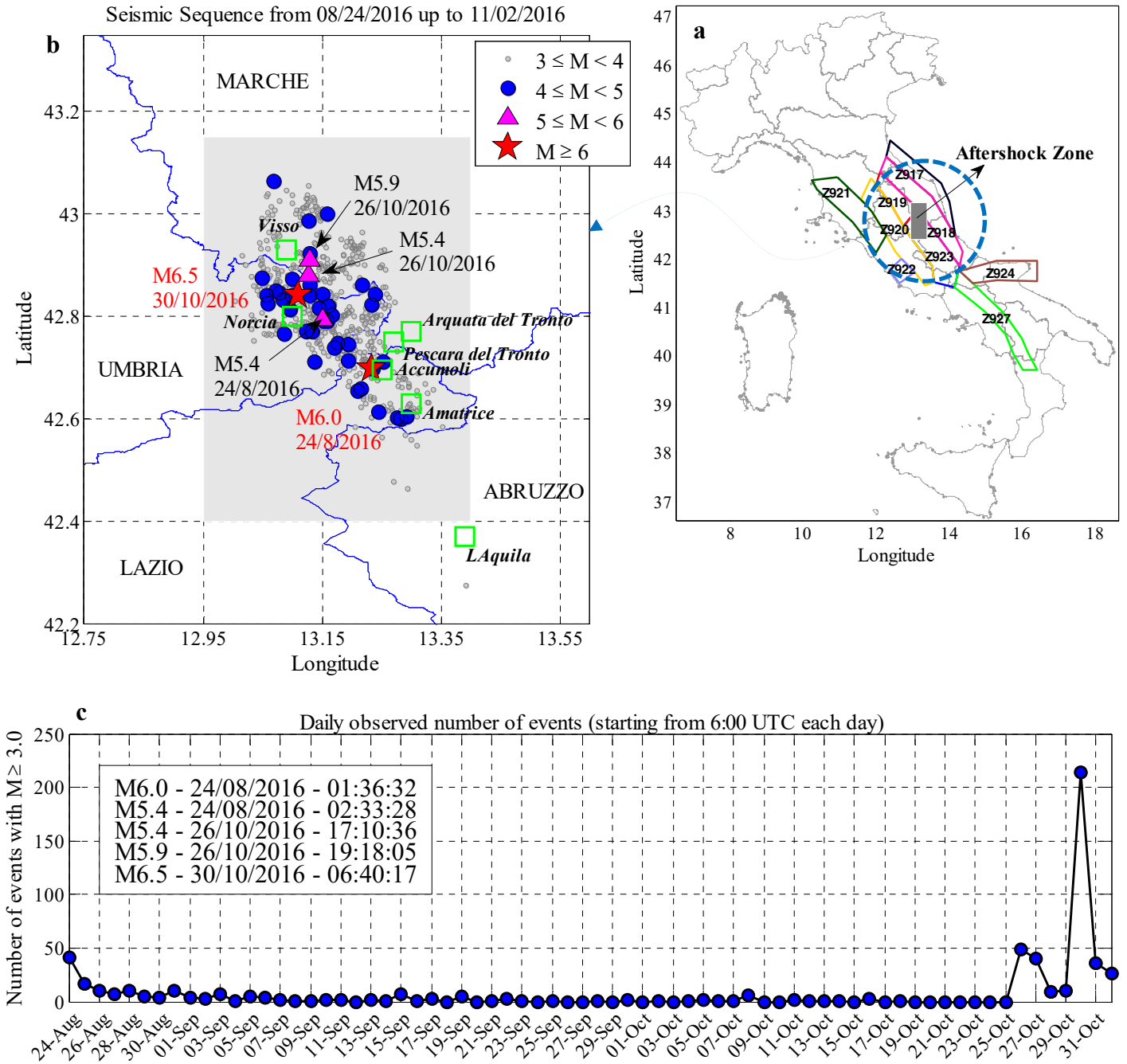
Figure 3: Amatrice-Norcia 2016 seismic sequence: (a) The aftershock zone indicated by the grey-coloured box in perspective with the surrounding Italian seismogenic zonation; (b) The spatial distribution of aftershock events based on Catalogue from August 24, 2016 (01:36 UTC) up to November 2, 2016 (10:32 UTC) bordering four neighbouring provinces in Italy. The grey-coloured box defines the considered aftershock zone and the most damaged towns are highlighted with green boxes. The main seismic events are illustrated as follows: M6.0 and M6.5 with red stars; M5.4 (24/08/16), M5.4 (26/10/16), M5.9 (26/10/16) with magenta triangles; aftershocks M≥3.0 with grey circles. (c) The number of events (with M≥3.0) in Catalogue occurred within a 24-hour interval starting from 6:00 UTC of the desired day.

The MCMC procedure for updating the model parameters is carried out adaptively (the evolution in the statistics (mean and COV) of model parameters $\theta=[\beta, K, K_t, K_R, c, p, d, q]$ are illustrated and discussed in [18]). The earthquakes of interest occurred within the correspond-

ing forecasting interval are illustrated as coloured dots (distinguished by magnitude). The two main events of the sequence with $M \geq 5.0$ (see also Figure 3) are identified with coloured stars (these events are shown for reference only and they did not necessarily take place in the illustrated map's corresponding forecasting interval). We also report the forecasted daily probabilities of having earthquakes of magnitude equal to or larger than $m=4$, 5 and 6 in the whole aftershock zone (see [18]).

At the right-hand side of each sub-figure, the observed (shown as a red star) vs. forecasted number of events (shown in an error-bar format) is illustrated for events with $M_l=3.0$ for the entire aftershock zone. The error-bar for the forecasted number of events features: the median value (the 50th percentile, equivalent of the logarithmic mean in the arithmetic scale) inside a grey-filled square, the (logarithmic) mean plus/minus one (logarithmic) standard deviation indicating the interval between 16th and 84th percentiles (marked with blue horizontal lines), and the (logarithmic) mean plus/minus two (logarithmic) standard deviations indicating the interval between 2nd and 98th percentiles (marked with black horizontal lines). This is done to help in locating the observed number of events within plus or minus certain number of standard deviations from the mean estimate. It can be seen that the observed number of events lies within plus/minus one standard deviation of the mean estimate.
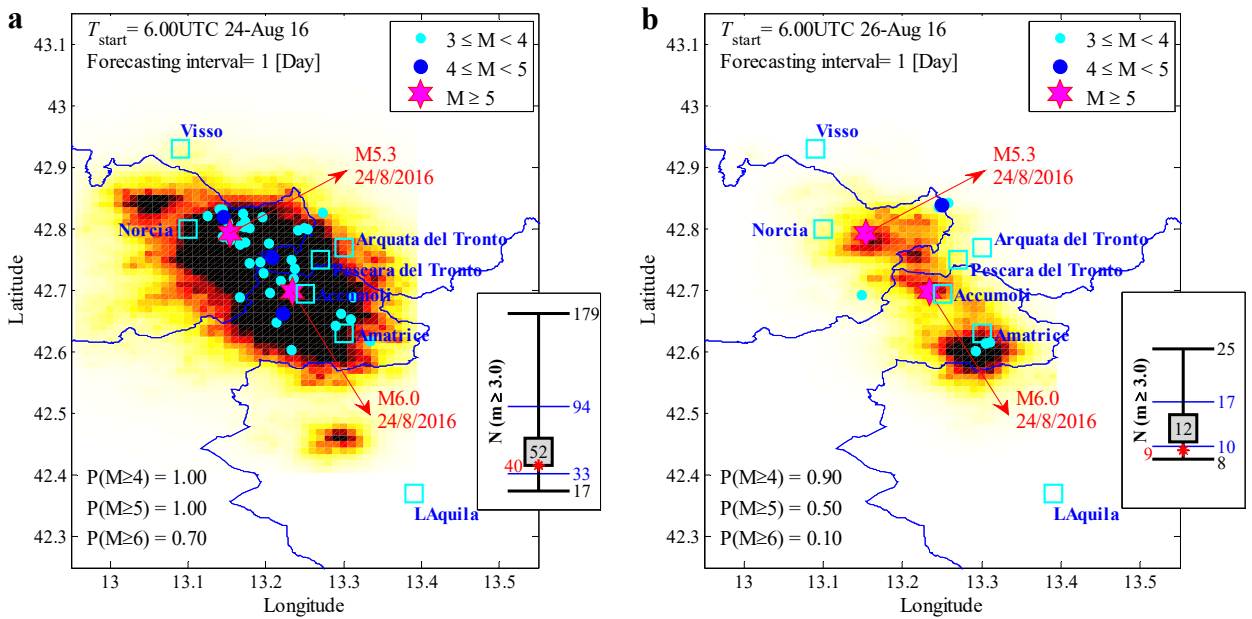
Figure 4: Forecasted vs. observed seismicity distribution in the aftershock zone after the event with Mw 6.0 at 01:36 UTC of 24/08/2016; the maps report the mean + 2 standard deviation confidence interval for the number of events per [km²] (latitude/longitude cells of a $0.01° \times 0.01°$ grid) equal to or greater than magnitude $M_l=3$ in the indicated 24-hour forecasting time window. The sub-figures illustrate the observed (plotted in red star) vs. the error-bar for the forecasted number of events with $m \geq M_l$ corresponding to the forecasting time interval: the median value (the 50th percentile, equivalent of the logarithmic mean in the arithmetic scale) inside a grey-filled square, the (logarithmic) mean plus/minus one (logarithmic) standard deviation indicating the interval between 16th and 84th percentiles (marked with blue horizontal lines), and the (logarithmic) mean plus/minus two (logarithmic) standard deviations indicating the interval between 2nd and 98th percentiles (marked with black horizontal lines)

3.3 Daily forecasts of seismicity from October 26 up to October 29

As mentioned before, on 26th of October, a Mw 5.4, followed within a two-hour delay by a Mw 5.9 earthquake (at 17:10 and 19:18 UTC, respectively), took place in the east of town Visso (located in the north-western part of the aftershock zone, see Figure 1a). This triggered a new aftershock sequence within the ongoing one. At this stage, given the time elapsed from the occurrence of the mainshock (i.e., around two months), it seemed quite tedious to consider all the events of interest up to the time of origin (i.e., 24th of August) for each forecasting interval. To achieve this (i.e., avoid considering all the events back to 24th of August), we performed a shift in the time of origin T_o from August 24th to 17:10 UTC of October 26th (time of occurrence of the Mw 5.4 earthquake, see Figure 3). After the occurrence of the event with Mw 5.4 at 17:10 UTC of 26/10/2016, we provide a 6-hour prediction of seismicity for the forecasting interval starting from T_{start} set to 18:00 UTC of 26/10/2016 (i.e., 50 minutes after the occurrence of Mw 5.4 event). At this point, we performed a shift in the time of origin by setting T_o to 17:10 UTC of 26th of October (see Figure 4).
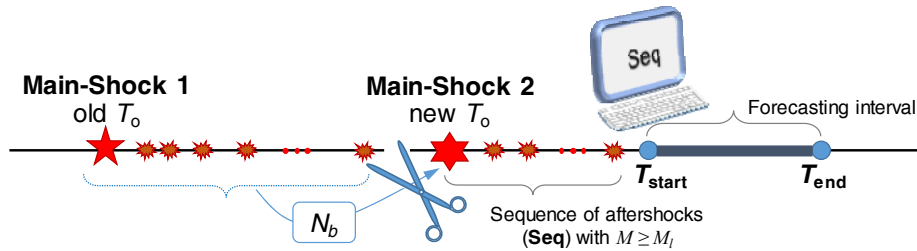
Figure 5: Schematic sketch of the shift in the time of origin T_o

The sequence **seq** includes all the triggered events with $M \geq 3$ occurred after 17:10 UTC of 26/10/2016 (including the main Mw 5.4 event). It should be noted that the event Mw 5.4 was not preceded by any foreshocks (i.e., no $M \geq 3$ events took place between 06:00 UTC and 17:10 UTC of 26 of October). Given the very low seismic activity prior to the major event and given the presence of very few events in **seq**, we did not perform Bayesian updating on the model parameter θ and used the statistics issued for 26/10/2016 (see [18]). It is important to note that the forecasted seismicity for the 24-hour interval elapsed after 06:00 UTC of October 26 is used herein (after proportioning it to a 6-hour forecasting interval) as the background seismicity $N_b(x,y,m|M_l)$. The background seismicity usually considers the long-term seismicity in the calculations and was assumed to be equal to zero in our previous calculations for the first part of the sequence staring from 24th of August. Herein, we use this background seismicity to conservatively approximate the triggering effect of the events occurred in the first part of the sequence (from August 24th to October 26th). The background seismicity is added as a constant term to the contribution of the triggering events (see Section 2). The forecasted seismicity map in terms of the mean plus two standard deviation for the number of events with $M \geq 3.0$ is shown in Fig. 6a. Observed events with $M \geq 3.0$ (coloured dots) occurred within the corresponding 6-hour forecasting interval are also highlighted on the map. The main two events with Mw 5.4 at 17:10 UTC assigned as the main-shock and the Mw 5.9 event at 19:18 UTC (which lies within the 6-hour forecasting interval) are shown with magenta stars. According to the right-hand side error-bar plot of Fig. 6a, the total number of registered events within the 6-hour forecasting interval (red star) is significantly higher than the forecasted values. This can be attributed to very few number of observed input data in **seq** for preforming the robust estimation and to the fact that model parameters were not tuned to the

newly triggered sequence. Although less successful in predicting the number of events, the model predicts exceedance probabilities $P(M \geq 5)$ and $P(M \geq 6)$ to be very high.

After the occurrence of the event with Mw 5.9 at 19:18 UTC, the seismicity forecast is provided in Fig. 6b again for the interval starting from 20:00 UTC (42 minutes after the Mw 5.9 event) up to 24:00 UTC of 26/10/2016 (i.e., a 4-hour time interval). The corresponding **seq** includes all the events with $M \geq 3.0$ which occurred (including the main event of Mw 5.4 at 17:10 UTC and Mw 5.9 at 19:18 UTC) after 17:10 UTC up to the starting time (20:00 UTC) of October 26. The model parameters θ are updated based on the information provided by the sequence **seq** with M_l set to 2.5 (see [18]). Note that the cut-off magnitude lower than 3.0 is assigned only for model updating purposes to gain more data and the seismicity rate is later calculated with $M_l = 3.0$. Fig. 6b illustrates the forecasted seismicity map in terms of the mean plus two standard deviation for the number of events with $M \geq 3.0$ within the 4-hour forecasting interval. Note that for the 4-hour time interval, the exceedance probabilities $P(M \geq 5)$ and $P(M \geq 6)$ increase in Fig. 6b after the occurrence of the event with Mw 5.9 at 19:18 UTC (compared to Fig. 6a). In addition, the observed number of events within the 4-hour time interval (sub-figure) lies within the plus/minus one standard deviation confidence interval.
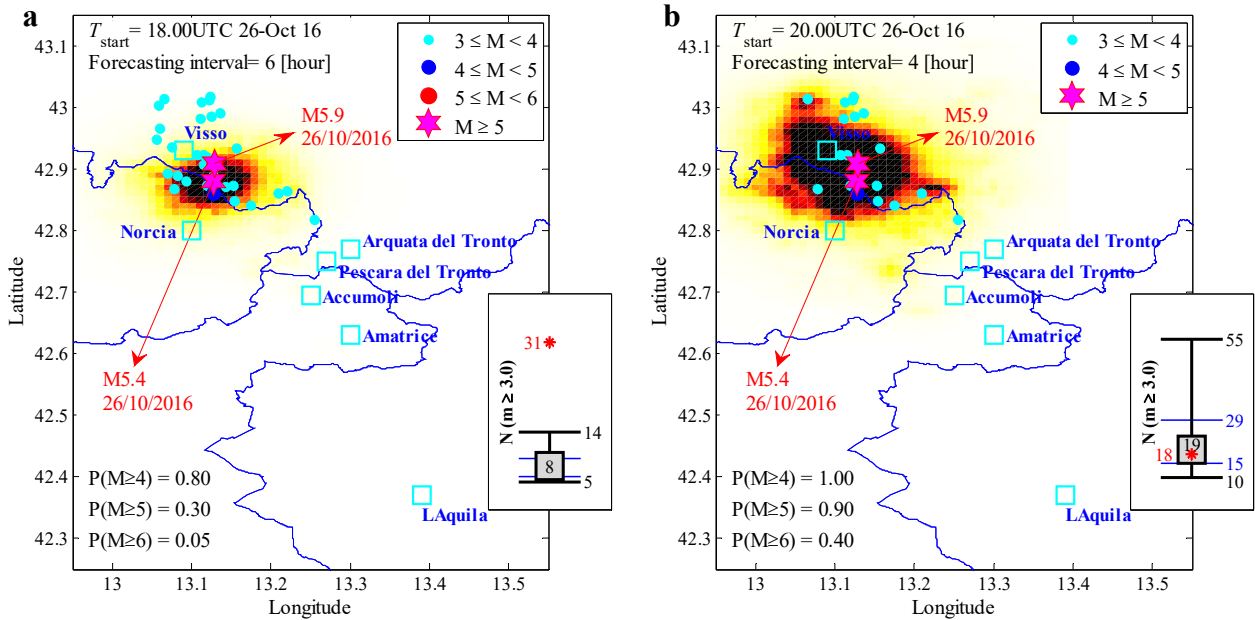
Figure 6: Forecasted vs. observed seismicity distribution in the aftershock zone after the event with Mw 5.4 at 17:10 UTC of 26/10/2016

3.4 Daily forecasts of seismicity from October 30 up to November 1

As mentioned before, on 30th of October, a Mw 6.5 event occurred in the North of Norcia at 6:40 UTC (located in the north-western part of the aftershock zone, see Figure 3). The first forecasting is performed for the same day of 30/10/2016 with T_{start} set to 12:00UTC and T_{end} set to 06:00 UTC of 31/10/2016 (i.e., 18-hour interval). At this stage, we performed a shift in the time of origin T_o from 17:10 UTC of 26th of October to 6:40 UTC of 30th of October. The background seismicity $N_b(x,y,m|M_l)$ is set (and proportioned to an 18-hour interval) to that of 30th of October for a 24-hour interval with starting time set to 6:00 UTC (see [18]). Fig. 7a

shows the map of forecasted seismicity with the back-drop of events occurred in this interval. The error-bar plot for the forecasted number of events manages to capture the observed number of events within one standard deviation confidence interval.

To measure the effect of the shift in the time of origin, the same forecasting presented in Fig. 7a is performed with time of origin set to 17:40 UTC of 26th of October. Fig, 7b shows the forecasted map of seismicity and the error-bar for the predicted number of events. The forecasted number of events are slightly lower than those predicted in the previous step in Figure 5c (after shifting the time of origin). This is to be expected since the latter forecast employs a time-invariant background seismicity to consider the events of interest occurred in the time interval between 17:10 UTC of 26th of October and 6.40 UTC of 30th of October. This is while the former forecast explicitly considers the triggering contribution of these events and the associated time-decay. Overall, it is reassuring to note that the two forecasts provide essentially the same information.
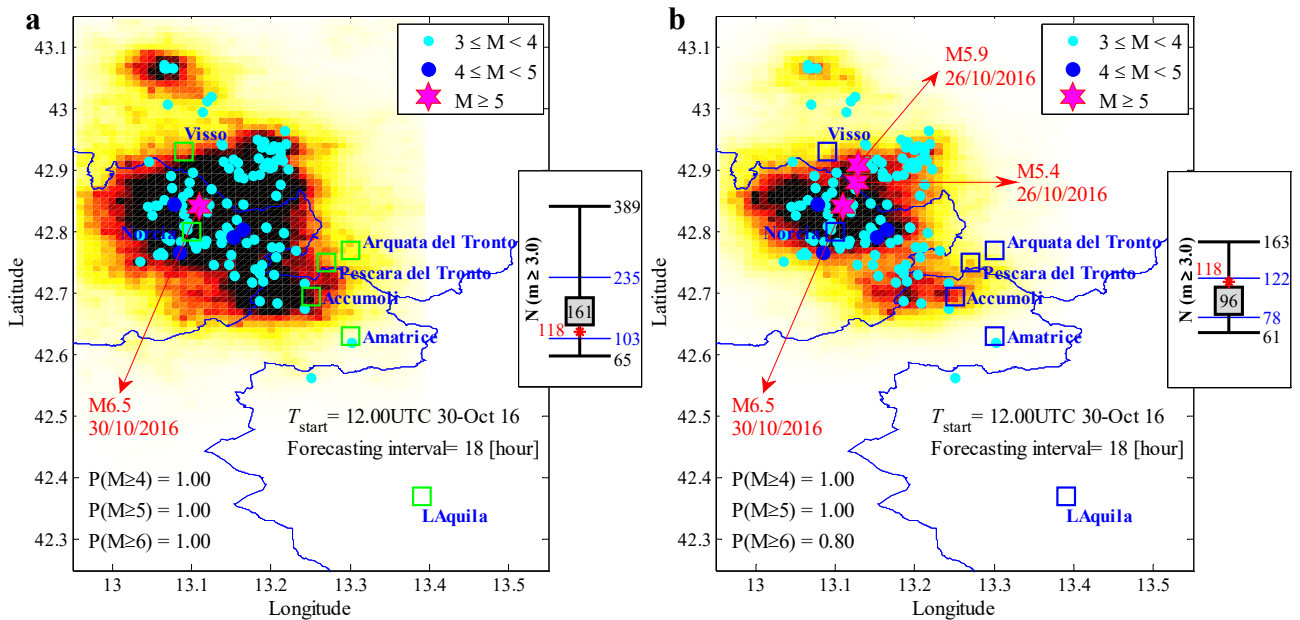
Figure 7: Forecasted vs. observed seismicity distribution in the aftershock zone after the event with Mw 6.5 at 6:40 UTC of 30/10/2016

3.5 Discussion on the results

It is observed that after an initial transition time (in the order of few hours, enough to accumulate enough events for updating the model parameters), the model quickly tunes into the sequence and provides forecasting that is reliable in most cases up to plus/minus one standard deviations. As expected, the procedure falls short of predicting the "main-shock" of 24th of October (17:10 UTC) as it happened when the sequence had decayed. The procedure, however, did a better job for forecasting the events occurred at 19:18 UTC of 26th of October and on 6.40 UTC of 30th October. This relative success can be attributed to the fact that these events took place at the initial stages of the newly triggered sequence of 26th of October when the seismic activity was still very high. The estimated model parameters present some time-dependent fluctuations but after a certain number of days elapsed after the main event, they

seem to stabilize. In general, the first sub-sequence (Mw 6 "mainshock" occurred at 1:36 UTC 24th of August) seems to be the mildest one in terms of the time decay in seismicity and is the least active in terms of sequence's productivity. The second sub-sequence (Mw 5.4 "mainshock" occurred at 17:10 UTC 26th of October) is intermediate both in terms of the rate of time-decay and the productivity. The third sub-sequence (Mw 6.5 "mainshock" occurred at 6:40 UTC 30th of October) has the steepest time-decay of seismicity and is the most active in terms of the productivity of the sequence.

4   CONCLUSIONS

- A fully simulation-based procedure is proposed for (a) Bayesian model updating of an epidemiological-type aftershock spatio-temporal clustering model; (b) robust operational forecasting of the number of events of interest expected to happen in each time frame.

- The robust forecasting considers the uncertainty (i.e., the joint probability distribution) in the model parameters.

- The model updating and forecasting procedure is carried on without human interference and use of expert judgement. The model is simply "tuning-in" automatically into the sequence of observed events.

- The choice of the recent Central Italy sequence of events as a demonstration of this procedure proved to be very challenging. This is because the sequence embedded three "sub-sequences" with different productive and decaying properties. We used the peculiarities of this sequence to test several different strategies for forecasting.

- To perform early forecast within an ongoing seismic sequence, a shift in the time of origin of the sequence is proposed by conservatively introducing a constant background seismicity (calculated by the procedure). This shift proved to be quite useful as it relieved us from the burden of summing up the triggering properties of all the events that took place in the previous "sub-sequence" (or the previous part of the sequence as we may wish to call it) at the small price of neglecting the time-decay in their triggering contribution.

- The proposed procedure for robust forecasting is conditioned on the available catalogue of events and the epidemiological model adopted for capturing the spatio-temporal aftershock clustering.

REFERENCES

[1]   M.C. Gerstenberger, S. Wiemer, L.M. Jones, P.A. Reasenberg. Real-time forecasts of tomorrow's earthquakes in California. *Nature*, **435**, 328-331, 2005.

[2]   T. H. Jordan, L. M. Jones. Operational earthquake forecasting: Some thoughts on why and how. *Seism. Res. Lett.*, **81**, 4, 571-574, 2010.

[3] T. H. Jordan, W. Marzocchi, A. J. Michael, M. C. Gerstenberger. Operational earthquake forecasting can enhance earthquake preparedness. *Seism. Res. Lett.*, **85**, 5, 955-959, 2014.

[4] W. Marzocchi, A.M. Lombardi, E. Casarotti. The establishment of an operational earthquake forecasting system in Italy. *Seism. Res. Lett.*, **85**, 5, 961-969, 2014.

[5] Y. Ogata. Statistical models for earthquake occurrences and residual analysis for point processes. *J. Am. Stat. Assoc.* **83**, 9-27, 1988.

[6] Y. Ogata. Space-time point-process models for earthquake occurrences. *Ann. Inst. Statist. Math.* **50**, 2, 379-402, 1998.

[7] T. A. Utsu. statistical study of the occurrence of aftershocks. *Geophys. Mag.* **30**, 521-605, 1961.

[8] W. Marzocchi, A. M. Lombardi. Real-time forecasting following a damaging earthquake. *Geophys. Res. Lett.* **36**, 2009.

[9] J. Zhuang, Y. Ogata, D. Vere-Jones. Stochastic declustering of space-time earthquake occurrences. *J. Am. Stat. Assoc.*, **97**, 458, 369- 380, 2002.

[10] Y. Ogata, J. Zhuang. Space–time ETAS models and an improved extension. *Tectonophysics* **413**, 1, 13-23, 2006.

[11] A. Veen, F. P. Schoenberg. Estimation of space-time branching process models in seismology using an EM-type algorithm. *J. Am. Stat. Assoc.* **103**, 614-624, 2008.

[12] E. Lippiello, F. Giacco, L. de Arcangelis, W. Marzocchi, C. Godano. Parameter Estimation in the ETAS Model: Approximations and Novel Methods. *Bull. Seism. Soc. Am.* **104**, 2, 985-994, 2014.

[13] A. M. Lombardi. (2015). Estimation of the parameters of ETAS models by Simulated Annealing. *Sci. Rep.*, **5**, 8417, 2015.

[14] F. Jalayer, D. Asprone, A. Prota, G. Manfredi, A decision support system for post-earthquake reliability assessment of structures subjected to aftershocks: an application to L'Aquila earthquake, 2009. *Bulletin of Earthquake Engineering*, **9** (4), 997-1014, 2011.

[15] H. Ebrahimian, F. Jalayer, D. Asprone, A.M. Lombardi, W. Marzocchi, A. Prota, G. Manfredi. Adaptive Daily Forecasting of Seismic Aftershock Hazard. *Bulletin of Seismological Society of America*, **104** (1),145-161, 2014.

[16] F. Jalayer, H. Ebrahimian. MCMC-based Updating of an Epidemiological Temporal Aftershock Forecasting Model. *Vulnerability, Uncertainty, and Risk*, 2093-2103; DOI 10.1061/9780784413609.210, 2014.

[17] T. Omi, Y. Ogata, Y. Hirata, K. Aihara. Intermediate-term forecasting of aftershocks from an early aftershock sequence: Bayesian and ensemble forecasting approaches. *J. Geophysical Res: Solid Earth*, **120**, 4, 2561-2578, 2015.

[18] H. Ebrahimian, F. Jalayer. Robust seismicity forecasting based on Bayesian parameter estimation for epidemiological spatio-temporal aftershock clustering models. *Scientific Reports, Nature*, **7**(9803), 1-15, 2017.

[19] J. L. Beck, S. K. Au. Bayesian updating of structural models and reliability using Markov Chain Monte Carlo simulation. *J. Eng. Mech. ASCE* **128**, 4, 380-391, 2002.

[20] H. Ebrahimian, F. Jalayer, D. Asprone, A.M. Lombardi, W. Marzocchi, A. Prota, G. Manfredi. An outlook into time-dependent aftershock vulnerability assessment. *4th ECCOMAS Thematic Conference on Computational Methods in Structural Dynamics and Earthquake Engineering (COMPDYN2013)*, M. Papadrakakis, V. Papadopoulos, V. Plevris (eds.), Kos Island, Greece, 12-14 June, 2013.

[21] H. Ebrahimian, F. Jalayer, D. Asprone, A.M. Lombardi, W. Marzocchi, A. Prota, G. Manfredi, A performance-based framework for adaptive seismic aftershock risk assessment. *Earthquake Engineering and Structural Dynamics*, **43** (14), 2179-2197, 2014.

[22] F. Jalayer, H. Ebrahimian, Seismic risk assessment considering cumulative damage due to aftershocks. *Earthquake Engineering and Structural Dynamics*, **46** (3), 369–389, 2017.

[23] F. Jalayer, I. Iervolino, G. Manfredi. Structural modeling uncertainties and their influence on seismic assessment of existing RC structures. *Struct. Saf*, **32**, 3, 220-228, 2010.

[24] N. Metropolis, A. W. Rosenbluth, M. N. Rosenbluth, A. H. Teller, E. Teller. Equations of state calculations by fast computing machines. *J. Chem. Phys.*, **21**(6), 1087-1092, 1953.

[25] W. K. Hastings. Monte-Carlo sampling methods using Markov chains and their applications. *Biometrika*, **57**(1), 97-109, 1970.

[26] Gruppo di Lavoro. *Redazione della mappa di pericolosità sismica prevista dall'Ordinanza PCM 3274 del 20 marzo 2003*. Rapporto Conclusivo per il Dipartimento della Protezione Civile, INGV, Milano-Roma, April 2004: 65 pp. + 5 appendixes (in Italian).